ChemPubSoc Europe

DOI: 10.1002/chem.201801251

CHEMISTRY A European Journal Full Paper

NMR Spectroscopy

Efficiency of Water-Soluble Nitroxide Biradicals for Dynamic Nuclear Polarization in Rotating Solids at 9.4 T: bcTol-M and cyolyl-TOTAPOL as New Polarizing Agents**

Michel-Andreas Geiger[+],[a] Anil P. Jagtap[+],[b] Monu Kaushik[+],[c] Han Sun,[a] Daniel Stöppler,[a] Snorri T. Sigurdsson,*[b] Björn Corzilius,*[c] and Hartmut Oschkinat*[a]

Abstract: Nitroxide biradicals are very efficient polarizing agents in magic angle spinning (MAS) cross effect (CE) dynamic nuclear polarization (DNP) nuclear magnetic resonance (NMR). Many recently synthesized, new radicals show superior DNP-efficiency in organic solvents but suffer from insufficient solubility in water or glycerol/water for biological applications. We report DNP efficiencies for two new radicals, the water-soluble **bcTol-M** and **cyolyl-TOTAPOL**, and include a comparison with three known biradicals, **TOTAPOL**, **bcTol**, and **AMUPol**. They differ by linker groups, featuring either a 3-aminopropane-1,2-diol or a urea tether, or by the structure of the alkyl substituents that flank the nitroxide groups. For evaluating their performances, we measured both signal enhancements ε and DNP-enhanced sensitivity κ, and compared the results to electron spin relaxation data recorded at the same magnetic field strength (9.4 T). In our study, differences in DNP efficiency correlate with changes in the nuclear polarization dynamics rather than electron relaxation. The ratios of their individual ε and κ differ by up to 20%, which is explained by starkly different nuclear polarization build-up rates. For the radicals compared here empirically, using proline standard solutions, the new radical **bcTol-M** performs best while being most soluble in water/glycerol mixtures.

Introduction

Dynamic nuclear polarization is a powerful method for increasing signal-to-noise ratios in MAS NMR,[1] and has recently enabled investigations in biomedical research or material science that otherwise would be inaccessible due to the lack of sensitivity.[2] DNP is based on the transfer of the large electron spin polarization to nuclear spin levels, driven by continuous microwave (MW) irradiation. Polarization is transferred via the solid effect (SE),[3] the Overhauser effect (OE)[4] or the cross effect (CE)[5] mechanisms, depending on the experimental conditions such as the type of polarizing agent and the magnetic field strength. At 9.4 T and around 100 K, the CE has proven to be most efficient. It mediates polarization transfer within a 3-spin system of two dipolar-coupled electrons and one hyperfine-coupled nucleus if the EPR spectrum of the radical is inhomogeneously broadened by *g* (Zeeman) anisotropy, showing a breadth (Δ) larger than the nuclear Larmor frequency (ω), and if a possible match between the difference of the two electron frequencies and the nuclear Larmor frequency can be achieved ($|\omega_{e1}-\omega_{e2}| = \omega_n$).[6] Nitroxide biradicals are well suited for CE DNP because these conditions are fulfilled, and at

[a] *M.-A. Geiger,[+] Dr. H. Sun, D. Stöppler, Prof. Dr. H. Oschkinat*
Leibniz-Forschungsinstitut für Molekulare Pharmakologie
Robert Roessle-Str. 10
13125 Berlin (Germany)
E-mail: oschkinat@fmp-berlin.de

[b] *Dr. A. P. Jagtap,[+] Prof. Dr. S. T. Sigurdsson*
Department of Chemistry, Science Institute
University of Iceland
Dunhaga 3
107 Reykjavik (Iceland)
E-mail: snorrisi@hi.is

[c] *Dr. M. Kaushik,[+] Dr. B. Corzilius*
Institut für Physikalische und Theoretische Chemie
Institut für Biophysikalische Chemie
und Biomolekulares Magnetresonanzzentrum (BMRZ)
Goethe-Universität Frankfurt
Max-van-Laue-Str.7-9
60438 Frankfurt am Main (Germany)
E-mail: corzilius@em.uni-frankurt.de

[+] *These authors contributed equally to this work.*

[**] *Abbreviations used in this manuscript for the radicals:* ***TEMPO*** *= 2,2,6,6-Tetramethylpiperidinyloxyl;* ***bcTol*** *= [bis(spirocyclohexyl-TEMPO-alcohol)urea];* ***bcTol-M*** *= bis(spirocyclohexyl-TEMPO-alcohol)-ureadimethyl;* ***TOTAPOL*** *= 1-(TEMPO-4-oxy)-3-(TEMPO-4-amino) propan-2-ol;* ***cyolyl-TOTAPOL*** *= [spirocyclohexanolyl-1-(TEMPO-4-oxy)-3-(TEMPO-4-amino) propan-2-ol];* ***AMUPol****: (15-{[(7-oxyl-3,11-dioxa-7-azadispiro[5.1.5.3]hexadec-15-yl)carbamoyl][2-(2,5,8,11-tetraoxatridecan-13-ylamino)}-[3,11-dioxa-7-azadispiro[5.1.5.3]hexadec-7-yl])oxidanyl;* ***BTnE****: bis-TEMPO-*n*-ethylene oxide;* ***bTbK****: bis-TEMPO-bis-ketal;* ***bTbtk-py****: bis-TEMPO-bis-thioketal-tetratetrahydropyran;* ***TEKPOL****: bis-phenylcyclohexyl-TEMPO-bis-ketal;* ***PyPol****: (15-{[(7oxyl-3,11-dioxa-7-azadispiro[5.1.5.3]hexadec-15-yl)carbamoyl]amino}-[3,11-dioxa-7-azadispiro[5.1.5.3]hexadec-7-yl])oxidanyl);* ***PyPol-diMe****: (15-{[(7oxyl-3,11-dioxa-7-azadispiro[5.1.5.3]hexadec-15-yl)carbamoyl]amino}-[3,11-dioxa-7-azadispiro[5.1.5.3]hexadec-7-yl])oxidanyl)-dimethyl.*

Supporting information and the ORCID identification number(s) for the author(s) of this article can be found under: https://doi.org/10.1002/chem.201801251.

the same time the homogeneous linewidth (δ) remains small ($\delta < \omega < \Delta$).

There have been systematic attempts to develop efficient polarizing agents for CE DNP by varying substituents or the linker of nitroxide biradicals,[7] with **BTnE**[8] and **TOTAPOL**[9] as prominent examples from the Griffin group. This stimulated interest in understanding the major factors determining radical performance, such as the effective electron–electron couplings, hyperfine couplings, as well as electron and nuclear relaxation times. The effective electron–electron coupling between the radical centers of the polarizing agents is essential for CE. It is composed of two contributions, the exchange interaction, J_{ex}, and the dipolar coupling. The exchange interaction is mediated by overlap of the spin-bearing molecular orbitals and appears only when the radical centers are separated by not more than a few chemical bonds and when favorable molecular geometries exist. In contrast, the dipolar coupling is a through-space interaction and depends directly on the distance between the paramagnetic centers and the orientation of their connecting vector with respect to the external magnetic field (B_0).

Since, the mutual orientation of the two *g* tensors of the interacting electrons plays an important role in CE efficiency, a rigid linker enforcing a favorable geometry may be advantageous.[6a,b] For example, a bisketal tether was used to connect the nitroxide moieties in the **bTbK** biradical to lock the relative orientation of the two radicals.[7c] Further important parameters are the electron spin relaxation times, because efficient DNP transfer depends on the selective saturation of EPR transitions, but also on the sufficient recovery of electron spin polarization for dynamic polarization of typically 1000 nuclear spins per electron. For this reason, functional groups influencing relaxation have been a focus in radical development. In **bTbtk-py**, for example, the methyl groups adjacent to the nitroxide groups have been replaced by six-membered spirotetrahydropyran rings to increase both solubility and electron spin relaxation times.[7f] Further examples, where the geminal methyl groups are substituted by spirocyclohexyl rings, are the bulky nitroxide biradicals **bCTbK** and **TEKPol** that show improved DNP efficiency at temperatures up to 200 K.[10] In recent years, it was shown that biradicals of the **PyPol**[11] series that have urea-based linkers yield high enhancements and excellent signal-to-noise ratios in biomolecular applications, in particular the water-soluble **AMUPol**[11] and **bcTol** (Figure 1).[12] Their excellent performance in DNP experiments makes them currently the radicals of choice for polarizing biological samples at 9.4 T and 100–200 K.

In an attempt to improve **bcTol** further and to understand factors determining radical efficiency, we synthesized two new radicals, **cyolyl-TOTAPOL** and the highly water-soluble **bcTol-M** (Figure 1). Their DNP performance as well as EPR properties were compared with **TOTAPOL**, **AMUPol** and **bcTol**. The molecular structures of the five radicals contain either **TOTAPOL**-type (3-aminopropane-1,2-diol) linkers or urea-based linkers, as well as different substitutions in the immediate vicinity of the nitroxide groups within the six-membered rings (i.e., methyl, spirotetrahydropyran, and spirocyclohexanolyl).

The analysis of the entire process of all steps of the polarization transfer from electrons to carbons via protons is very complex and experimentally challenging. In the course of this work a selected set of the relevant parameters were determined. In order to assess the DNP performance of each radical empirically, we determined both the $^{1}H–^{13}C$ cross polarization (CP) signal enhancement factors, in addition to the signal-to-noise ratios per 10 min of data acquisition on a proline standard sample under microwave irradiation (SNR_{ON}), applying typical measurement conditions. This allowed direct comparison of our results with many DNP MAS NMR studies that have reported the predominantly used enhancement factor (i.e., MW_{ON} compared to MW_{OFF}). The measurements reported here also provide the more practically relevant sensitivity measure, which takes care of MAS-induced nuclear depolarization that lowers the nuclear polarization for MW_{OFF} as well as effects of nuclear relaxation, signal bleaching and DNP build-up behavior. Thus, this measure displays eventually the net signal gain[13] effective in CP NMR experiments. In the course of our analysis, a molecular mechanics-based conformational search was performed to explore the conformational space adopted by the radicals, in an attempt to correlate electron–electron distance distributions of the biradicals with DNP performance. Nuclear and electron spin relaxation parameters were determined at the same magnetic field strength (9.4 T) and temper-

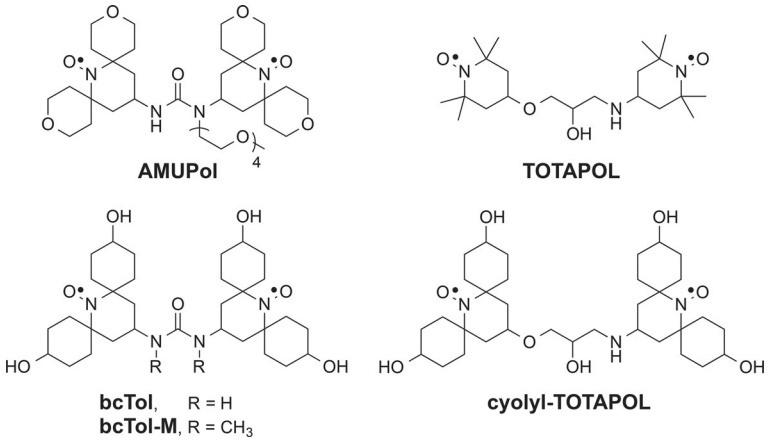

Figure 1. Structures of **AMUPol**, **TOTAPOL**, **bcTol**, **bcTol-M**, and **cyolyl-TOTAPOL**.

ature (110 K). Our results suggest that the improvement in DNP efficiency of urea-based biradicals cannot be correlated with their electron relaxation parameters but rather with the size of the effective electron–electron coupling and effects on nuclear polarization build-up rate, which may be influenced by the presence of methyl groups at the linker.

Experimental Section

Sample preparation for EPR and DNP-enhanced MAS NMR experiments

The biradical samples for EPR measurements were prepared in a solution containing 60% [D_8]glycerol, 30% D_2O and 10% H_2O (GDH). This stock was then aliquoted and to each fraction the respective polarizing agent was added to yield 10 mM final biradical concentration (i.e., 20 mM in unpaired electrons). Each solution was transferred to a quartz capillary (0.3 mm outer diameter).

Samples for DNP-enhanced NMR measurements were made from a similar stock containing 0.35 M ^{13}C,^{15}N-proline in GDH. This stock was then aliquoted and to each fraction the respective polarizing agent was added to yield 10 mM final biradical concentration (i.e., 20 mM in unpaired electrons). Each solution was transferred to a 3.2 mm ZrO_2 rotor (Bruker) with a volume of 25 μL per sample.

EPR spectroscopy

A 263 GHz Bruker EleXsys E780 spectrometer was used for all EPR measurements. The spectrometer uses a Bruker Ascent DNP magnet (89 mm) centered at 9.40 T with a superconducting sweep coil. The sweep coil can be charged from −20 A to +20 A, corresponding to a nominal range of ±75 mT change in magnetic field. The power supply is remotely controlled by the Bruker Xepr software used for data acquisition. The spectrometer is equipped with a custom-built resonator (with up to 5 kHz modulation frequency) operating in TE_{011} mode. Microwave power of about 15 mW was used for all experiments in pulsed mode. During field sweep experiments the rate of change in field was kept small so that magnetic field induced by the sweep coil is linear with change in current. Sweep width and number of points were chosen accordingly to follow constant sweep rate for each experiment. Sample and probe temperature was maintained (at 110 K) with a helium-flow cryostat from Oxford Instruments.

Echo-detected (ED) field-sweep EPR spectra were recorded by the Hahn echo pulse sequence shown in Figure S12. The magnetic field was swept at the rate of 0.05 mT s^{-1}. Pulse lengths and delay times (τ) were optimized for each sample for maximum intensity of symmetric echo. Length of $\pi/2$ pulse was chosen between 50 and 60 ns and τ was varied between 380 ns and 420 ns. From these ED-EPR spectra, pseudo-cw (continuous wave) spectra were calculated using the Easyspin package for MATLAB.[14] The predefined function 'fieldmod'[14] was applied to the ED field-sweep spectra of each radical with a pseudo-modulation amplitude of 0.5 mT.

Echo decay curves for the measurement of the phase-memory time constant (T_{2e}) were also recorded by using the Hahn echo pulse sequence. The magnetic field was set to the spectral positions corresponding to g_{xx}, g_{yy}, g_{zz}, or in between those principal axis positions. T_{2e} was extracted from thus obtained relaxation curves as discussed in the Supporting Information.

The longitudinal electronic relaxation (T_{1e}) was measured using the saturation recovery pulse sequence shown in Figure S13. A pulse train with a picket-fence pattern consisting of 29 ($\pi/2$) pulses was used to saturate the EPR signal. The interpulse delay time between saturation pulses was about twice or thrice T_{2e}. A Hahn echo detection sequence was applied after a variable delay time (t). T_{1e} was extracted from the experimental curves by determining the build-up time constant from bi-exponential fits and also by mathematically extracting the time required for the saturation factor to decay between e^{-2} and e^{-3} as discussed in the Supporting Information.

In order to ensure correct assignments of field positions for measurement of relaxation time constants care was taken that the echo intensity was recorded while the field was incrementally swept between different field points. This allowed for alignment of field-dependent relaxation measurements and the field-swept ED EPR spectra despite the hysteresis of the superconducting sweep unit.

DNP-enhanced NMR spectroscopy

All DNP experiments were conducted at 9.4 T (400 MHz), using a wide bore magnet with a Bruker Avance III console. Continuous wave microwave irradiation was supplied through the attached 263 GHz gyrotron (≈5 Watt). All spectra were processed with Topspin 3.0 (Bruker). All data were recorded under similar CP conditions with a ^1H–^{13}C cross polarization step. All reported signal-to-noise values refer to the CO signal intensity of proline. For each sample, the CP conditions were optimized for maximum signal intensity. The signal-to-noise after 10 minutes of data acquisition (SNR_{ON}) was determined with the SINO command in Topspin (see Supporting Information). Spectral width was chosen to be wide enough to minimize the error on the noise and as narrow as required to avoid vicinity to signals, for example due to spinning side bands. Proton T_{1H} values were measured using an inversion recovery experiment for each sample. The recycling delay was set to $1.3 \times T_{1H}$ for maximum sensitivity. All samples were measured at 8 kHz MAS at 110 K in a Bruker cryo-MAS DNP probe.

Molecular mechanics-based conformational search

Energy minimization and conformational search were carried out for all radicals by MacroModel integrated in Maestro V11.0 (Schrödinger Inc.). The OPLS3 force field[15] with the implicit GB/SA water solvent model was employed.[16] The initial structures of the radicals were generated manually. They were subsequently energy-minimized to a convergence threshold of 0.05 kJ $(mol\,Å)^{-1}$ in at most 2500 iterations. As there is no free radical atom type for oxygen in MacroModel, all oxygen radi-

cals were replaced by hydroxyl groups. The energy-minimized structures were further used as the starting structures for the conformational search, where the mixed torsional/low-mode sampling method was applied. All the conformers generated with a 20.92 kJ mol^{-1} energy window were kept, except that redundant conformers were eliminated using a root-mean-squared-distance (RMSD) cutoff of 0.5 Å.

Results

Synthesis of bcTol-M and cyolyl-TOTAPOL

Synthesis of **bcTol-M** started with the protected spirocyclohexanolyl nitroxide **1**, which was used for the synthesis of **bcTol**.[12] Reductive amination of **1** with methylamine gave amino methyl derivative **2** in good yields. Treatment of **2** with triphosgene, followed by deprotection of the hydroxyl groups, yielded **bcTol-M** as a yellow crystalline solid (Scheme 1).

Synthesis of **cyolyl-TOTAPOL** was carried out in similar manner to that of the reported procedure for **TOTAPOL**.[9] Reduction of the carbonyl group of **1** yielded hydroxyl derivative **4**, which was alkylated with epichlorohydrin to give epoxy derivative **5** in good yields (Scheme 2). Coupling of amino derivative **6**[12] with **5**, followed by deprotection of the hydroxyl groups, yielded **cyolyl-TOTAPOL** as a yellow crystalline solid.

bcTol-M showed excellent solubility in water (170 mM). The solubility in GDH (60% [D_8]glycerol, 30% D_2O, 10% H_2O) was even higher (250 mM) which is eight times higher than for **AMUPol** (30 mM)[11] and 1.6 times higher than **bcTol** (150 mM).[12] To the best of our knowledge, **bcTol-M** has by far the highest water-solubility among all known nitroxide-based biradicals. It is also noteworthy that **bcTol-M**, similarly to **bcTol,**[12] dissolves immediately without sonication.[11] Furthermore, both biradicals are crystalline solids that are easy to handle. The solubility exhibited by **cyolyl-TOTAPOL** is similar to the parent biradical **TOTAPOL** in GDH (15 mM).[17]

EPR spectra of radicals at 263 GHz

Pseudo-continuous wave (CW) EPR spectra at 263 GHz of all five biradicals are shown in Figure 2. Overall, the Zeeman ani-

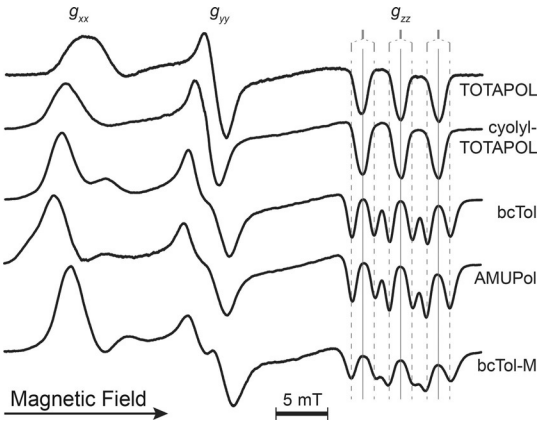

Figure 2. Pseudo-modulated CW EPR spectra at 110 K recorded at 263 GHz. Spectra are vertically shifted for better visual comparison to compensate for variation in resonant microwave frequency.

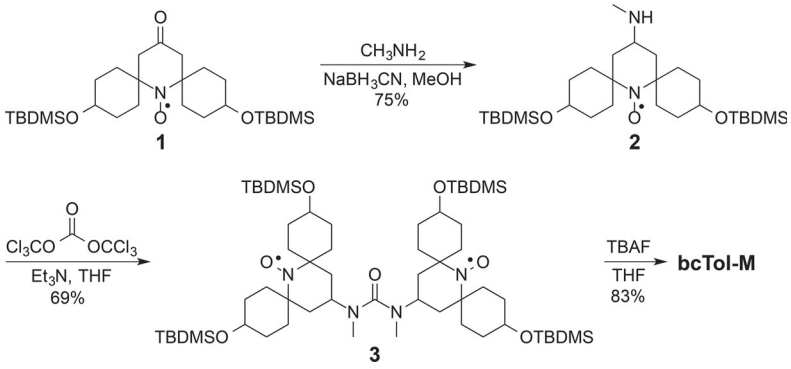

Scheme 1. Synthesis of **bcTol-M**.

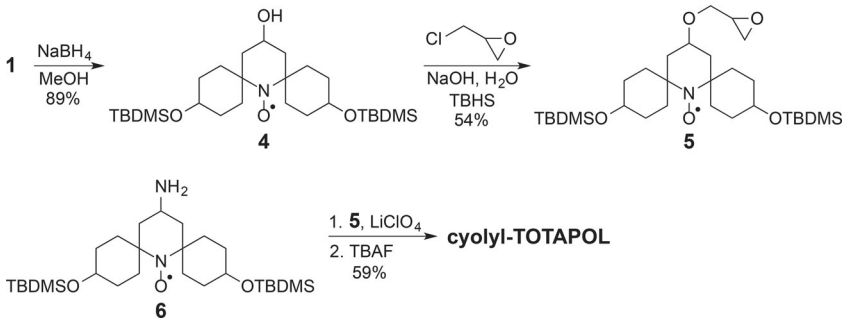

Scheme 2. Synthesis of **cyolyl-TOTAPOL**.

sotropy dominates the spectral shape. At the high-field edge, corresponding to g_{zz}, a further splitting into a triplet is visible due to the hyperfine interaction with ^{14}N ($I=1$). In addition, a resolved intramolecular, effective electron–electron coupling is visible as splitting in g_{zz}, and g_{yy} peaks for **bcTol**, **AMUPol**, and **bcTol-M**. This coupling is caused by the relatively close distance of nitroxide moieties (dipolar contribution) imposed by the short urea bridging element as well as by an exchange interaction J_{ex} mediated through the molecular orbital system.[18]

Electron spin relaxation at 263 GHz

Figure 3 shows T_{1e} (saturation) and T_{2e} (echo) decay curves obtained at the field position close to the MW irradiation position under typical DNP conditions (field position C in Figure S14). The relaxation time constants were determined from the decay curves and are compared in Table 1, together with the often-discussed saturation factor $T_{1e}T_{2e}$. A detailed description of how the decay curves were calculated and how the time constants were extracted are shown in the Supporting Information.

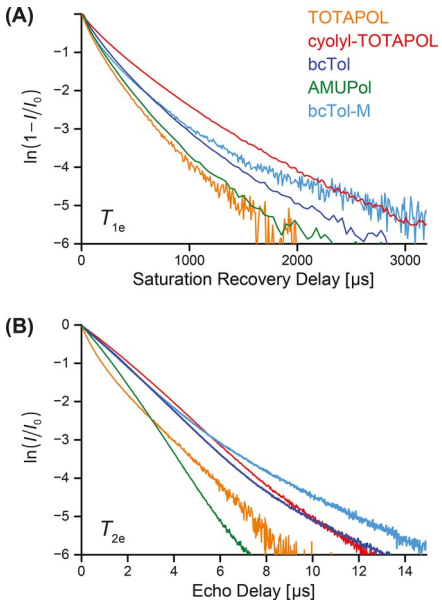

Figure 3. Decay curves recorded at 110 K at spectral feature corresponding to DNP condition for (A) longitudinal relaxation (T_{1e}) and (B) transverse relaxation (T_{2e}). Starting polarization is normalized to unity, as explained in the Supporting Information.

Table 1. Electron relaxation times T_{1e}, T_{2e}, and electron saturation factor for each biradical, measured at a temperature of 110 K and the approximate spectral position where MAS DNP is typically performed. The relaxation parameters are extracted directly from decay curves (see text and Figure 3).

Biradical	T_{1e} [µs]	T_{2e} [µs]	$T_{1e}T_{2e}$ [µs^2]
TOTAPOL	283	0.904	256
cyolyl-TOTAPOL	526	2.076	1092
bcTol	394	1.854	730
AMUPol	309	1.33	411
bcTol-M	437	1.827	798

When varying the magnetic field position, it was observed that for each biradical the relaxation time constants varied significantly along the spread of the EPR spectra (Figure S15). Figure 4 shows this effect explicitly along the ED EPR line shape for **cyolyl-TOTAPOL** and **bcTol-M**. At 110 K, T_{2e} is typically shortest at the g_{yy} position and increases towards the edges of the anisotropic spectrum. In contrast, T_{1e} monotonically increases from the low towards the high field edge. This variation of relaxation parameters can be attributed to a large anisotropy of relaxation and we expect that it significantly contributes to the DNP process. Since the spectral position of spin packets evolves constantly during sample rotation for CE DNP under MAS, the electron spin relaxation parameters vary equally during a rotor period. The ramifications of this situation are very difficult to predict and may range from a simple averaging of the effective relaxation time constant to a strong influence of the instantaneous relaxation properties during different steps of the MAS CE mechanism. While the former situation seems to be most probable in the case of T_{1e} (i.e., one nitroxide experiencing an average T_{1e} over the full rotor period) due to the rotation period being several-fold shorter than measured T_{1e} constants, the instantaneous T_{2e} probably has to be taken in to account for various CE matching events. However, the relative variation over the full EPR spectral breadth for T_{2e}

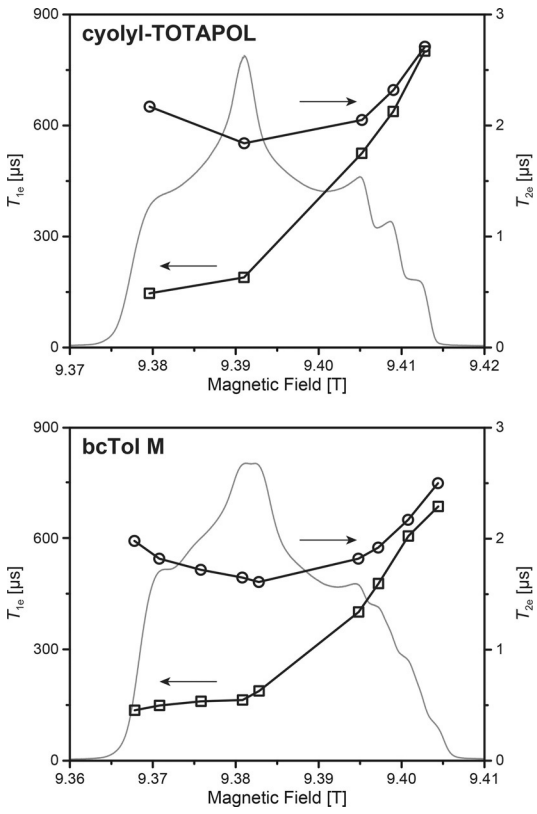

Figure 4. Relaxation trends with magnetic field: T_{1e} (open square, shown on left ordinate) and T_{2e} (open circle, shown on right ordinate) vary in magnitude along the echo-detected EPR spectrum (gray line) shown exemplarily for **cyolyl-TOTAPOL** and **bcTol-M** recorded at 110 K.

(≈40%) is much smaller than that of T_{1e} (up to 400%). Nevertheless, this anisotropy has not yet been accounted for in numerical simulations of MAS CE DNP and it will be interesting to see if it has a significant effect in the prediction of enhancement factors or DNP field profiles.[19]

DNP efficiency

The efficiency of the five radicals was compared via polarization of proline in a solution of the standard cryoprotecting solvent, "GDH" (60% [D_8]glycerol, 30% D_2O, 10% H_2O), using the same stock solution for the preparation of the five samples. As is common in solid-state NMR at low spinning frequencies, 1D ^{13}C NMR spectra were recorded with an individually optimized ^{1}H–^{13}C CP. Control experiments showed that the line widths of proline carbon resonances are independent of temperature and radical after freezing. Two different types of parameters were determined: (i) the DNP enhancement factor ε, measured by comparing peak intensities in spectra recorded with and without MW irradiation but otherwise identical conditions (Figure 5, light blue columns), and (ii) the sensitivity κ which is defined as the signal-to-noise ratio under microwave irradiation divided by the square root of the total measurement time,[20] in our case chosen to be 10 minutes [Eq. (1)].

$$\kappa = \frac{\mathrm{SNR}}{\sqrt{N_{sc}\cdot 1.3\cdot T_{1H}}} \quad (1)$$

In all such experiments, the recycle delay was set to a sample-specific $1.3\times T_{1H}$, and the number of scans (N_{SC}) was adjusted accordingly. Please note that for reasons of simplicity we use T_{1H} as symbol for both the nuclear spin-lattice relaxation time and the DNP build-up time constant. For the radical-doped samples, these parameters are equal.

The enhancement factor reports largely on the efficiency of electron–nuclear transfer processes which are driven by differential electron saturation and mediated by the hyperfine coupling as well as electron–electron couplings. The measurement of SNR_{ON} displays the actual sensitivity, thus also reflecting the effects of nuclear depolarization and other factors such as the efficiency of CP and the rate of nuclear polarization build-up. To ensure comparability, both types of measurements were always performed subsequently for each radical, immediately after freezing the sample, temperature equilibration, tuning and parameter optimization, and within a time segment of an hour. In this way we employed the same optimized parameters for CP, recycle delay, and decoupling, thus strongly reducing the possibility for divergent results due to systematically different experimental conditions. The measured values are listed in Table 2 and graphically displayed in Figure 5 (A). The two radicals with **TOTAPOL**-type linkers are shown to the left in Figure 5 and the three urea-based radicals to the right. For the latter series, the degree of amide alkylation increases from left to the right.

Overall, the three radicals with a urea-derived linker performed similarly and significantly better than **cyolyl-TOTAPOL** and especially **TOTAPOL**, which correlates with the larger effective electron–electron couplings of the former group of radicals (Figure 2). **TOTAPOL** is outperformed despite its largest sensitivity in MW_{OFF} experiments, showing the smallest depolarization/quenching by a significant margin. Within the series of urea-based radicals, there is a larger variation in the SNR_{ON} and κ than in the enhancement values. An interesting case is given by the direct comparison between **bcTol** and **bcTol-M**, where the only difference is the alkylation level of the bridging amides. Here, the enhancement of **bcTol-M** is only 5% larger,

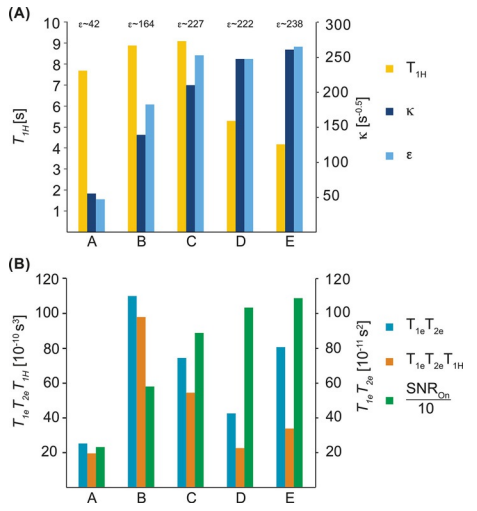

Figure 5. DNP efficiency of the biradicals and their relaxation parameters. (A) Sensitivity (steel blue), proton longitudinal build-up rate T_{1H} (yellow), enhancement values ε, (bright blue). (B) Signal-to-noise per 10 min divided by 10 $SNR_{ON}/10$ (green), saturation (cyan blue) and relaxation (orange) factors. (A: **TOTAPOL** B: **cyolyl-TOTAPOL** C: **bcTol**, D: **AMUPol**, E: **bcTol-M**).

Table 2. Signal-to-noise ratio (SNR) per 10 min, enhancement ε and sensitivity values κ recorded at 110 K and 8 kHz MAS under CW microwave irradiation. The five different proline samples are doped with 10 mM nitroxide biradicals. Data was evaluated for ^{1}H–^{13}C CP experiments, (all reported SNR values refer to the CO signal of proline.

Radical	SNR_{ON}	SNR_{OFF}	ε	κ [$s^{-0.5}$]	N_{sc}	T_{1H} [s]	Rel. polarization gain [arb. units]
TOTAPOL	1351±52	38±5	42±2	55±2	60	7.7	43.2±6.3(1.7)
cyolyl-TOTAPOL	3447±8	21±2	164±3	141±1	52	8.9	118±17(0)
bcTol	5358±193	26±2	227±8	220±8	60	7.8	171±25(6)
AMUPol	6079±94	28±1	222±9	247±4	88	5.3	160±23(3)
bcTol-M	6463±386	30±1	238±7	264±14	110	4.2	152±23(9)
no radical	13±2	14±2	–	0.56±0.08	12	40	1

whereas the sensitivity gain is increased by 17% owing to the decrease of T_{1H} by **bcTol-M**.

By normalizing SNR_{ON} to the number of scans, and dividing it by the normalized SNR_{OFF} of the proline sample without radical, we obtain ratios that are a measure of the DNP-induced change in proton polarization monitored at the proline carbon sites, see last column in Table 2 where we call them 'relative polarization gain'. This ratio reflects the virtual gain in proton polarization as detected via transfer to the analyte carbon signals, whereas the absolute gain in proton polarization is certainly higher but influenced by paramagnetic quenching, CP efficiency, etc. With the assumption that the Boltzmann polarization at 110 K is 0.0087%, we may express this ratio as virtual polarizations of 0.38, 1.03, 1.49, 1.39, and 1.32% for radicals A, B, C, D, and E, respectively. Interestingly, bcTol shows the highest virtual polarization, however, SNR_{ON} is higher for bcTol-M than for bcTol through T_{1H} effects.

In Figure 5(B), the DNP-enhanced signal-to-noise ratios are shown together with the respective saturation ($T_{1e}T_{2e}$) and relaxation factors ($T_{1e}T_{2e}T_{1H}$). While the saturation factor accounts for the continuous wave saturation efficiency, the latter parameter has been discussed as a potential measure of cross effect efficiency.[7a] In general, a clear correlation between the relaxation parameters and the SNR_{ON} or enhancement values is not apparent. While the different T_{1H} values may explain the divergence between enhancements and SNR values, the electron relaxation parameters appear particularly uncorrelated to either one. According to Figure 5(B), **cyolyl-TOTAPOL** would be expected to perform best, while **AMUPol** would perform significantly worse than **bcTol**, if the enhancements would depend mostly on electron relaxation.

An insightful relation was revealed when the normalized SNR gain (i.e., SNR_{ON} of a radical-doped sample with MW irradiation compared to the SNR_{OFF} of an undoped sample) was plotted against the DNP enhancement factors (Figure 6). From a general perspective, an overall correlation is apparent. However, a closer look at the distribution reveals a considerable divergence from a straight line. For **cyolyl-TOTAPOL**, the enhancement values suggest 74% effectiveness in comparison to **AMUPol**, whereas it is in reality only 57% for the proline standard samples employed in this study as stated by the SNR_{ON} values. This divergence is particularly relevant when comparing the performance of **bcTol**, **AMUPol** and **bcTol-M**. The enhancement values of these radicals are similar, while the SNR_{ON} increase with the degree of alkylation and speak for **bcTol-M** as the radical of choice.

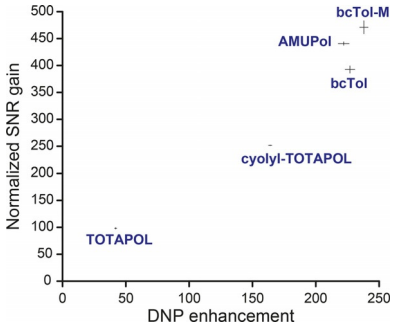

Figure 6. Correlation between the normalized SNR gain and the DNP enhancement factor ε.

Molecular mechanics-based conformational search

In an attempt to correlate the conformational space adopted by the biradicals with the EPR and DNP NMR data, molecular mechanics-based conformational searches were performed, using the OPLS3 force field in MacroModel employing an implicit solvent model (Figure 7). The results for the five biradicals differ with respect to the distribution of electron–electron distances and angles between the nitroxide groups. The 3-aminopropane-1,2-diol linker in **TOTAPOL** is longer than the urea-based linker, but is flexible, enabling distances even below 9 Å. The maximum distances between the nitroxides in **TOTAPOL** are around 16 Å, with a high occurrence of conformers in the range of 13–16 Å that contain many orientations of the nitroxide groups relative to each other. In contrast, the urea linker is short and either rigid or flexible, depending on the substitution pattern. In our simulations, the double bond character of the bond connecting the nitrogen to the carbonyl group in the urea linker depends critically on the presence of a proton as substituent on the nitrogen. If a urea nitrogen carries a proton, a conformational search utilizing the OPLS3 force field indicates that the rotation around the CO–N bond is hindered and the bond length is shortened in comparison to a doubly alkylated urea nitrogen. If the nitrogen does not carry a proton, the force field allows for free rotation around the CO–N bond and a considerable conformational space is occupied. Thus, the radical centers in the urea-linked radicals may adopt a minimum distance (d_{min}) of 9 Å but will not be further than 13 Å apart. There is a considerable difference in distribution, whereby **bcTol-M** allows shorter distances (down to 9 Å) with a spread of up to 11 Å, in comparison to the planar **bcTol** ($d_{min} > 12.2$ Å). **AMUPol** was expected to show free rotations around the CO–N bond involving the doubly alkylated urea nitrogen but appears more or less locked in a single conformation due to interactions of the first ethylene glycol chain oxygen with the urea amide group. However, the force field used may produce an overly constraint molecule. In all cases, the piperidine moiety may rotate around the connecting bond.

Discussion

Five different radicals, including the new radicals **cyolyl-TOTAPOL** and **bcTol-M**, were investigated at 9.4 T with respect to their EPR properties and DNP NMR efficiency. Their performance as polarization sources in DNP experiments was characterized by the enhancement factor ε as well as SNR_{ON} measurements using standard proline samples containing 10 mM biradical in GDH. The electron relaxation parameters for the radicals are very different, and difficult to correlate with the molecular structures of the biradicals. Furthermore, we do not see a clear correlation between electron relaxation properties and DNP performance.

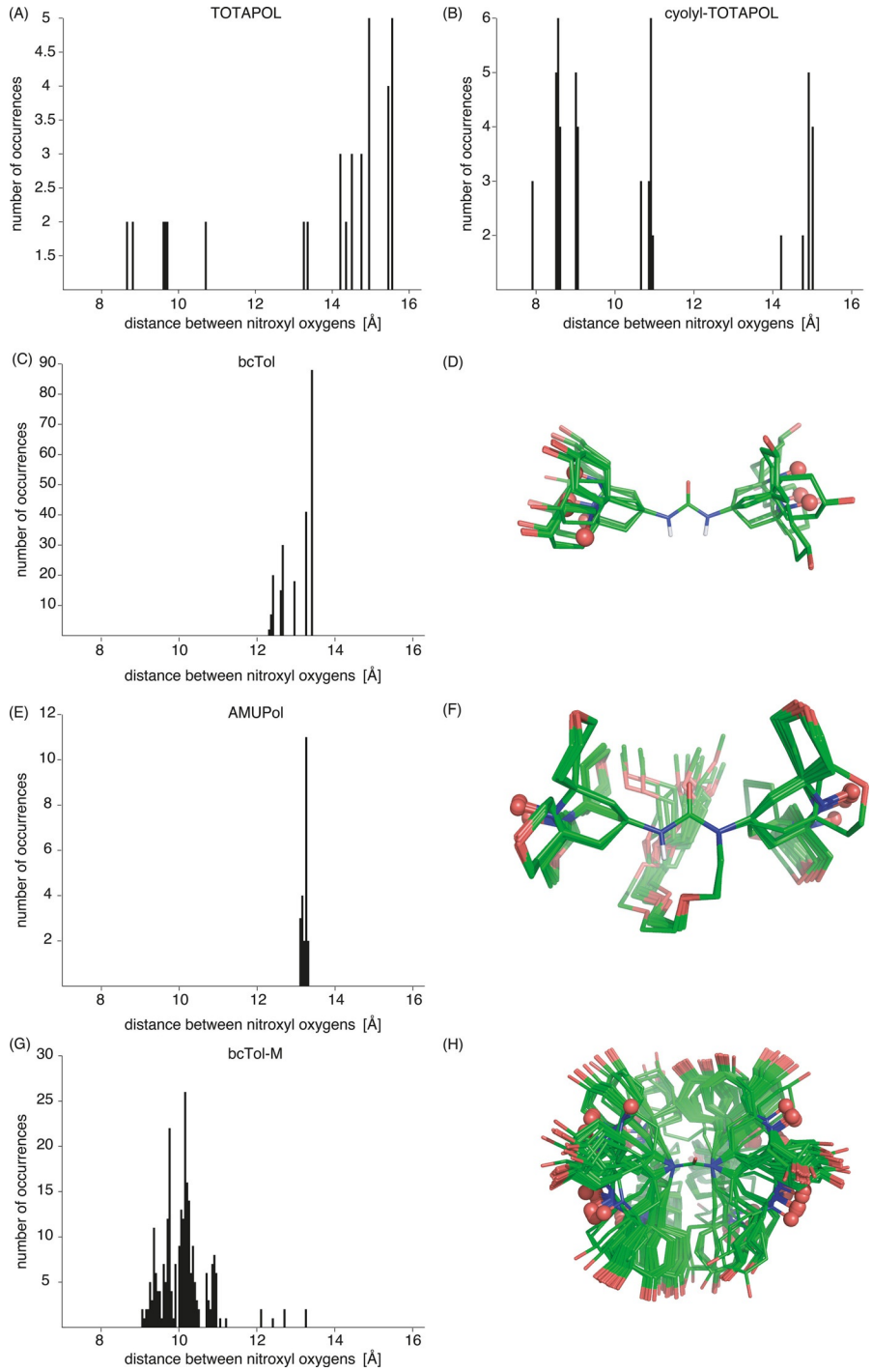

Figure 7. Distance distribution of the nitroxide oxygen atoms: conformational ensembles were calculated with molecular mechanics-based conformational search for the biradicals **TOTAPOL** (A), **cyolyl-TOTAPOL** (B), **bcTol** (C), **AMUPol** (E) and **bcTol-M** (G). Structural ensambles containing a number of favourable conformers are also shown for the radicals **bcTol** (D) **AMUPol** (F) and **bcTol-M** (H). The bin width of the histograms was set to 0.2 Å.

A clear correlation was, however, obtained between the two types of linkers and the DNP efficiency, whereby radicals with a urea moiety showed significantly higher enhancements and also SNR_{ON} than 3-aminopropane-1,2-diol-linked radicals. The two types of linkers give rise to different effective electron–electron dipolar couplings, largely through influences on the magnitude of J_{ex}[18] that is large for the urea-linked radicals, as manifested in additional splitting patterns in their EPR spectra (Figure 2, Table 1). As a second factor, their (average) electron–electron distances may be shorter, but not enough to explain the larger splitting. Within the series of urea-linked radicals, the increase in SNR_{ON} correlates with the number of substituents on the urea linker. This is a result of the change in proton polarization dynamics, connected to a shorter T_{1H} and thus DNP build-up time for **bcTol-M**. This is corroborated by the relative polarizations that are shown in the last column of

Table 2, which indicate a higher efficiency per scan for bcTol, however, its T_{1H} is much longer than that of bcTol-M. The structural differences between **bcTol** and **bcTol-M** are similar to the differences between the two radicals **PyPol** and **PyPol-diMe**.[7a] The better performance of **PyPol-diMe** has been attributed to the change of the relative orientation of the TEMPO moieties upon alkylation.[7b] Our molecular mechanics-based conformational search shows a random distribution of orientations for the dimethylated radical whereas extended, more ordered structures are observed in the non-methylated case.

Three of the biradicals under investigation here contain spirocyclohexanolyl groups that are adjacent to the nitroxide group. The influence of replacing the methyl groups as present in **TOTAPOL** with cyclohexanolyl rings has been discussed earlier.[10] Consistently with these earlier observations, **cyolyl-TOTAPOL** shows higher values for ε and κ than **TOTAPOL**. A strict comparison of the influences by the tetrahydropyran and spirocyclohexanolyl rings cannot be made on the basis of our data, but it is fair to say that both groups may lead to very similar DNP performance. An advantage of biradicals with the spirocyclohexanolyl rings, such as in **bcTol** and **bcTol-M** lies in the better solubility and easier handling of the compounds.

The molecular mechanics-based conformational search yielded insight into the accessible conformational space and flexibility of the various radicals and are correlated with the EPR spectra. Conformational inhomogeneity is displayed in the ^{14}N hyperfine triplet at the high-field edge of the EPR spectra (Figure 2), where the electron–electron interaction is directly represented as a further splitting of these lines. These g_{zz} components in the EPR spectra of the 3-aminopropane-1,2-diol-linked radicals show broader lines but no discernible doublet splitting, in contrast to those in the spectra of the urea-linked ones, correlating with the larger distribution of electron–electron distances observed in the molecular mechanics-based conformational search (Figure 7). Among the urea-linked radicals, **bcTol-M** shows a larger line width of the g_{zz} components than **bcTol** or especially **AMUPol**, again correlating with a wider distribution of electron–electron distances and a larger number of conformers observed in the molecular mechanics simulations.

Conclusions

In summary, we report the new radical **bcTol-M** with strongly improved solubility in water or glycerol/water that shows in our study large enhancements (>230) and also a high SNR_{ON} when used to polarize a proline standard sample. In SNR_{ON} measurements, its slightly better performance compared to other radicals is largely determined by an effect on the proton T_{1H} of the analyte. The exact mechanism is not clear; however, we note that the presence of the methyl groups that also promote nuclear relaxation might play an important role. Given the simplified handling of **bcTol-M**, which is a crystalline solid, we consider it an ideal tool for biological studies. In particular, its high solubility in water and glycerol/water mixtures enables highly concentrated stock solutions to be prepared, which significantly simplifies sample preparation.

Acknowledgements

This work was financially supported by the Icelandic Research Fund (141062051), by a doctoral fellowship to A.P.J. from the University of Icelandic Research Fund, and by the Deutsche Forschungsgemeinschaft (DFG) through Emmy Noether grant CO802/2-1 awarded to B.C.. Further support by BMRZ is acknowledged. Additionally, we acknowledge funding from the Deutsche Forschungsgemeinschaft: M.-A.G. via SFB 740 and D.S. via the SFB 1078 Project B1.

Conflict of interest

The authors declare no conflict of interest.

Keywords: dynamic nuclear polarization · magic angle spinning · NMR spectroscopy · radicals · water-soluble

[1] a) A. W. Overhauser, *Phys. Rev.* **1953**, *92*, 411 – 415; b) T. R. Carver, C. P. Slichter, *Phys. Rev.* **1953**, *92*, 212 – 213.

[2] a) A. Lesage, M. Lelli, D. Gajan, M. A. Caporini, V. Vitzthum, P. Miéville, J. Alauzun, A. Roussey, C. Thieuleux, A. Mehdi, G. Bodenhausen, C. Copéret, L. Emsley, *J. Am. Chem. Soc.* **2010**, *132*, 15459 – 15461; b) O. Lafon, A. S. L. Thankamony, T. Kobayashi, D. Carnevale, V. Vitzthum, I. I. Slowing, K. Kandel, H. Vezin, J.-P. Amoureux, G. Bodenhausen, M. Pruski, *J. Phys. Chem. C* **2013**, *117*, 1375 – 1382; c) F. Blanc, S. Y. Chong, T. O. McDonald, D. J. Adams, S. Pawsey, M. A. Caporini, A. I. Cooper, *J. Am. Chem. Soc.* **2013**, *135*, 15290 – 15293; d) U. Akbey, B. Altin, A. Linden, S. Ozcelik, M. Gradzielski, H. Oschkinat, *Phys. Chem. Chem. Phys.* **2013**, *15*, 20706 – 20716; e) A. J. Rossini, C. M. Widdifield, A. Zagdoun, M. Lelli, M. Schwarzwalder, C. Copéret, A. Lesage, L. Emsley, *J. Am. Chem. Soc.* **2014**, *136*, 2324 – 2334.

[3] a) E. Erb, J.-L. Motchane, J. Uebersfeld, *C. R. Hebd. Seances Acad. Sci.* **1958**, *246*, 2121 – 2123; b) M. Abraham, R. W. Kedzie, C. D. Jeffries, *Phys. Rev.* **1957**, *106*, 165 – 166; c) A. Abragam, W. G. Proctor, *C. R. Hebd. Seances Acad. Sci.* **1958**, *246*, 2253 – 2256.

[4] T. V. Can, M. A. Caporini, F. Mentink-Vigier, B. Corzilius, J. J. Walish, M. Rosay, W. E. Maas, M. Baldus, S. Vega, T. M. Swager, R. G. Griffin, *J. Chem. Phys.* **2014**, *141*, 064202.

[5] a) A. V. Kessenikh, V. I. Lushchikov, A. A. Manenkov, Y. V. Taran, *Phys. Solid State* **1963**, *5*, 321 – 329; b) C. F. Hwang, D. A. Hill, *Phys. Rev. Lett.* **1967**, *19*, 1011 – 1014; c) C. F. Hwang, D. A. Hill, *Phys. Rev. Lett.* **1967**, *18*, 110 – 112.

[6] a) F. Mentink-Vigier, U. Akbey, Y. Hovav, S. Vega, H. Oschkinat, A. Feintuch, *J. Magn. Reson.* **2012**, *224*, 13 – 21; b) K. R. Thurber, R. Tycko, *J. Chem. Phys.* **2012**, *137*, 084508; c) A. S. L. Thankamony, J. J. Wittmann, M. Kaushik, B. Corzilius, *Prog. Nucl. Magn. Reson. Spectrosc.* **2017**, *102 – 103*, 120 – 195.

[7] a) D. J. Kubicki, G. Casano, M. Schwarzwälder, S. Abel, C. Sauvée, K. Ganesan, M. Yulikov, A. J. Rossini, G. Jeschke, C. Copéret, A. Lesage, P. Tordo, O. Ouari, L. Emsley, *Chem. Sci.* **2016**, *7*, 550 – 558; b) C. Sauvée, G. Casano, S. Abel, A. Rockenbauer, D. Akhmetzyanov, H. Karoui, D. Siri, F. Aussenac, W. Maas, R. T. Weber, T. Prisner, M. Rosay, P. Tordo, O. Ouari, *Chem. Eur. J.* **2016**, *22*, 5598 – 5606; c) Y. Matsuki, T. Maly, O. Ouari, H. Karoui, F. Le Moigne, E. Rizzato, S. Lyubenova, J. Herzfeld, T. Prisner, P. Tordo, R. G. Griffin, *Angew. Chem. Int. Ed.* **2009**, *48*, 4996 – 5000; *Angew. Chem.* **2009**, *121*, 5096 – 5100; d) F. A. Perras, R. R. Reinig, I. I. Slowing, A. D. Sadow, M. Pruski, *Phys. Chem. Chem. Phys.* **2016**, *18*, 65 – 69; e) M. A. Geiger, M. Orwick-Rydmark, K. Marker, W. T. Franks, D. Akhmetzyanov, D. Stoppler, M. Zinke, E. Specker, M. Nazare, A. Diehl, B. J. van Rossum, F. Aussenac, T. Prisner, U. Akbey, H. Oschkinat, *Phys. Chem. Chem. Phys.* **2016**, *18*, 30696 – 30704; f) M. K. Kiesewetter, B. Corzilius, A. A. Smith, R. G. Griffin, T. M. Swager, *J. Am. Chem. Soc.* **2012**, *134*, 4537 – 4540.

[8] K.-N. Hu, H.-h. Yu, T. M. Swager, R. G. Griffin, *J. Am. Chem. Soc.* **2004**, *126*, 10844 – 10845.
[9] C. Song, K.-N. Hu, C.-G. Joo, T. M. Swager, R. G. Griffin, *J. Am. Chem. Soc.* **2006**, *128*, 11385 – 11390.
[10] A. Zagdoun, G. Casano, O. Ouari, M. Schwarzwalder, A. J. Rossini, F. Aussenac, M. Yulikov, G. Jeschke, C. Coperet, A. Lesage, P. Tordo, L. Emsley, *J. Am. Chem. Soc.* **2013**, *135*, 12790 – 12797.
[11] C. Sauvée, M. Rosay, G. Casano, F. Aussenac, R. T. Weber, O. Ouari, P. Tordo, *Angew. Chem. Int. Ed.* **2013**, *52*, 10858 – 10861; *Angew. Chem.* **2013**, *125*, 11058 – 11061.
[12] A. P. Jagtap, M. A. Geiger, D. Stoppler, M. Orwick-Rydmark, H. Oschkinat, S. T. Sigurdsson, *Chem. Commun.* **2016**, *52*, 7020 – 7023.
[13] a) F. Mentink-Vigier, S. Paul, D. Lee, A. Feintuch, S. Hediger, S. Vega, G. De Paepe, *Phys. Chem. Chem. Phys.* **2015**, *17*, 21824 – 21836; b) H. Takahashi, D. Lee, L. Dubois, M. Bardet, S. Hediger, G. De Paepe, *Angew. Chem. Int. Ed.* **2012**, *51*, 11766 – 11769; *Angew. Chem.* **2012**, *124*, 11936 – 11939.
[14] S. Stoll, A. Schweiger, *J. Magn. Reson.* **2006**, *178*, 42 – 55.
[15] E. Harder, W. Damm, J. Maple, C. Wu, M. Reboul, J. Y. Xiang, L. Wang, D. Lupyan, M. K. Dahlgren, J. L. Knight, J. W. Kaus, D. S. Cerutti, G. Krilov, W. L. Jorgensen, R. Abel, R. A. Friesner, *J. Chem. Theory Comput.* **2016**, *12*, 281 – 296.
[16] W. C. Still, A. Tempczyk, R. C. Hawley, T. Hendrickson, *J. Am. Chem. Soc.* **1990**, *112*, 6127 – 6129.
[17] W.-M. Yau, K. R. Thurber, R. Tycko, *J. Magn. Reson. Ser. A* **2014**, *244*, 98 – 106.
[18] P. Gast, D. Mance, E. Zurlo, K. L. Ivanov, M. Baldus, M. Huber, *Phys. Chem. Chem. Phys.* **2017**, *19*, 3777 – 3781.
[19] F. Mentink-Vigier, S. Vega, G. De Paepe, *Phys. Chem. Chem. Phys.* **2017**, *19*, 3506 – 3522.
[20] R. R. Ernst, G. Bodenhausen, A. Wokaun, *Principles of Nuclear Magnetic Resonance in One and Two Dimensions*, Oxford University Press **1990**, *1*, 61.

Manuscript received: March 12, 2018
Revised manuscript received: May 1, 2018
Accepted manuscript online: May 9, 2018
Version of record online: August 13, 2018